



AFRL-RX-WP-JA-2015-0188

**GROWTH OPTIMIZATION STUDIES TO DEVELOP
INAS/GAINSB SUPERLATTICE MATERIALS FOR
VERY LONG WAVELENGTH INFRARED DETECTION
(POSTPRINT)**

**H. J. Haugan, G. J. Brown, K. Mahalingam, and L. Grazulis
AFRL/RXAN**

**OCTOBER 2014
Interim Report**

Approved for public release; distribution unlimited.

See additional restrictions described on inside pages

STINFO COPY

© 2014 Elsevier B. V.

**AIR FORCE RESEARCH LABORATORY
MATERIALS AND MANUFACTURING DIRECTORATE
WRIGHT-PATTERSON AIR FORCE BASE, OH 45433-7750
AIR FORCE MATERIEL COMMAND
UNITED STATES AIR FORCE**

NOTICE AND SIGNATURE PAGE

Using Government drawings, specifications, or other data included in this document for any purpose other than Government procurement does not in any way obligate the U.S. Government. The fact that the Government formulated or supplied the drawings, specifications, or other data does not license the holder or any other person or corporation; or convey any rights or permission to manufacture, use, or sell any patented invention that may relate to them.

This report was cleared for public release by the USAF 88th Air Base Wing (88 ABW) Public Affairs Office (PAO) and is available to the general public, including foreign nationals.

Copies may be obtained from the Defense Technical Information Center (DTIC)
(<http://www.dtic.mil>).

AFRL-RX-WP-JA-2015-0188 HAS BEEN REVIEWED AND IS APPROVED FOR
PUBLICATION IN ACCORDANCE WITH ASSIGNED DISTRIBUTION STATEMENT.

//Signature//

GAIL J. BROWN
Nanoelectronic Materials Branch
Functional Materials Division

//Signature//

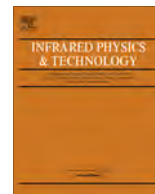
DIANA M. CARLIN, Chief
Nanoelectronic Materials Branch
Functional Materials Division

//Signature//

KAREN R. OLSON, Actg Chief
Functional Materials Division
Materials and Manufacturing Directorate

This report is published in the interest of scientific and technical information exchange, and its publication does not constitute the Government's approval or disapproval of its ideas or findings.

REPORT DOCUMENTATION PAGE			Form Approved OMB No. 074-0188	
Public reporting burden for this collection of information is estimated to average 1 hour per response, including the time for reviewing instructions, searching existing data sources, gathering and maintaining the data needed, and completing and reviewing this collection of information. Send comments regarding this burden estimate or any other aspect of this collection of information, including suggestions for reducing this burden to Defense, Washington Headquarters Services, Directorate for Information Operations and Reports, 1215 Jefferson Davis Highway, Suite 1204, Arlington, VA 22202-4302. Respondents should be aware that notwithstanding any other provision of law, no person shall be subject to any penalty for failing to comply with a collection of information if it does not display a currently valid OMB control number. PLEASE DO NOT RETURN YOUR FORM TO THE ABOVE ADDRESS.				
1. REPORT DATE (DD-MM-YYYY) October 2014		2. REPORT TYPE Interim		3. DATES COVERED (From – To) 17 January 2013 – 28 September 2014
4. TITLE AND SUBTITLE GROWTH OPTIMIZATION STUDIES TO DEVELOP INAS/GAINSB SUPERLATTICE MATERIALS FOR VERY LONG WAVELENGTH INFRARED DETECTION (POSTPRINT)		5a. CONTRACT NUMBER FA8650-11-D-5800-0006		
		5b. GRANT NUMBER		
		5c. PROGRAM ELEMENT NUMBER 62102F		
6. AUTHOR(S) H.J. Haugan, G.J. Brown, K. Mahalingam, and L. Grazulis		5d. PROJECT NUMBER 4348		
		5e. TASK NUMBER		
		5f. WORK UNIT NUMBER X0KY		
7. PERFORMING ORGANIZATION NAME(S) AND ADDRESS(ES) AFRL/RXAN Materials and Manufacturing Directorate Wright-Patterson Air Force Base, OH 45433-7750		8. PERFORMING ORGANIZATION REPORT NUMBER		
9. SPONSORING / MONITORING AGENCY NAME(S) AND ADDRESS(ES) Air Force Research Laboratory Materials and Manufacturing Directorate Wright Patterson Air Force Base, OH 45433-7750 Air Force Materiel Command United States Air Force		10. SPONSOR/MONITOR'S ACRONYM(S) AFRL/RXAN		
		11. SPONSOR/MONITOR'S REPORT NUMBER(S) AFRL-RX-WP-JA-2015-0188		
12. DISTRIBUTION / AVAILABILITY STATEMENT Approved for public release; distribution unlimited. This report contains color.				
13. SUPPLEMENTARY NOTES PA Case Number: 88ABW-2014-2725; Clearance Date: 05 June 2014. Journal article published in Journal of Infrared Physics & Technology (2015) 99-102. © 2014 Elsevier B. V. The U.S. Government is joint author of the work and has the right to use, modify, reproduce, release, perform, display or disclose the work. The final publication is available at http://dx.doi.org/10.1016/j.infrared.2014.09.016 .				
14. ABSTRACT In order to develop ternary antimonide-based superlattice (SL) materials for very long wavelength infrared (VLWIR) detection, systematic growth optimization studies were performed to produce high quality ternary materials. For the studies, a SL structure of 47.0 Å InAs/21.5 Å Ga _{0.75} In _{0.25} Sb was selected to create a very narrow band gap. Results indicate that an epitaxial process developed can produce a precisely controlled band gap around 50 meV, but the material quality of grown SL layers is particularly sensitive to growth defects formed during the growth process. Since Group III antisites and strain-induced dislocations are the dominant structural defects responsible for the low radiative efficiencies, our optimization strategies to eliminate these defects have focused on stabilizing III/V incorporation during surface reconstruction by manipulating the growth surface temperature and balancing the residual strain of the SLs by adjusting the As/Sb flux ratio. The optimized ternary SL materials exhibited an overall strong photoresponse over a wide wavelength range up to ~ 15 μm that is important for developing VLWIR detectors. A quantitative analysis of the lattice strain, performed at the atomic scale by aberration corrected transmission electron microscopy, provided valuable information about the strain distribution at the interfaces that was important for optimizing the strain balancing process during SL layer growth.				
15. SUBJECT TERMS superlattices, molecular beam epitaxy, infrared detector, antimonides				
16. SECURITY CLASSIFICATION OF:		17. LIMITATION OF ABSTRACT SAR	18. NUMBER OF PAGES 7	19a. NAME OF RESPONSIBLE PERSON (Monitor) Gail J. Brown
a. REPORT Unclassified	b. ABSTRACT Unclassified			c. THIS PAGE Unclassified



Growth optimization studies to develop InAs/GaInSb superlattice materials for very long wavelength infrared detection



H.J. Haugan*, G.J. Brown, K. Mahalingam, L. Grazulis

Air Force Research Laboratory, Materials and Manufacturing Directorate, Wright-Patterson Air Force Base, OH 45433, USA

ARTICLE INFO

Article history:

Received 14 July 2014

Available online 28 September 2014

Keywords:

Superlattices
Molecular beam epitaxy
Infrared detector
Antimonides

ABSTRACT

In order to develop ternary antimonide-based superlattice (SL) materials for very long wavelength infrared (VLWIR) detection, systematic growth optimization studies were performed to produce high quality ternary materials. For the studies, a SL structure of 47.0 Å InAs/21.5 Å Ga_{0.75}In_{0.25}Sb was selected to create a very narrow band gap. Results indicate that an epitaxial process developed can produce a precisely controlled band gap around 50 meV, but the material quality of grown SL layers is particularly sensitive to growth defects formed during the growth process. Since Group III antisites and strain-induced dislocations are the dominant structural defects responsible for the low radiative efficiencies, our optimization strategies to eliminate these defects have focused on stabilizing III/V incorporation during surface reconstruction by manipulating the growth surface temperature and balancing the residual strain of the SLs by adjusting the As/Sb flux ratio. The optimized ternary SL materials exhibited an overall strong photoreponse over a wide wavelength range up to ~15 μm that is important for developing VLWIR detectors. A quantitative analysis of the lattice strain, performed at the atomic scale by aberration corrected transmission electron microscopy, provided valuable information about the strain distribution at the interfaces that was important for optimizing the strain balancing process during SL layer growth.

© 2014 Elsevier B.V. All rights reserved.

1. Introduction

The InAs/GaInSb superlattice (noted as “ternary SL”) system provides several distinctive advantages suitable for very long wavelength infrared (VLWIR) detection [1]. With increasing indium composition, a very narrow band gap can be achieved with a smaller period for the ternary SL system, leading to a larger absorption coefficient due to enhanced electron and hole wavefunction overlap [2]. More importantly, the strain can create a large splitting between the heavy-hole and light-hole bands in the ternary SLs, which reduces the hole–hole Auger recombination process and increases the minority carrier lifetime, thus improving the device detectivity [3]. Despite these theoretical advantages, very few papers have examined the ternary SL growth processes in recent years and reported their device results to verify theoretically predicted performance limit. Recently, Haugan et al. [4,5] have shown that an excellent quality of the ternary materials can be processed using a molecular beam epitaxy (MBE) growth process specifically engineered for the ternary material growth. Their optimized SL materials can generate a strong photoreponse signal, a high mobility, and a long 300 K carrier lifetime. The 300 K carrier

decay time measured from their ternary SL materials extended up to ~84 ns, which is longer than the most reported 300 K lifetime values from processed SL detector materials [6,7].

In this report, using a combination of high-resolution X-ray diffraction (HRXRD), atomic force microscopy (AFM), and photoconductivity measurements, we continuously refined the MBE process and tuned growth conditions to produce the highest-quality ternary SL materials that can be used for VLWIR detection. Since most MBE-grown III–V heterostructures are affected by a large number of growth defects generated during surface reconstruction and strain balancing processes, we optimized the III/V stoichiometry by manipulating the growth surface condition, and engineered the interface composition to match the effective lattice constant of the SL to its substrate by adjusting As/Sb flux ratio. We used a SL structure of 47.0 Å InAs/21.5 Å Ga_{0.75}In_{0.25}Sb to create the band gap around 50 meV, and high-resolution transmission electron microscopy (HRTEM) to characterize the strain distribution at the interfaces.

2. Growth details

The InAs/GaInSb SL materials in this study were grown in a Varian MBE reactor equipped with dual-filament effusion cells for the

* Corresponding author.

Group III elements, and valved cracker cells for the Group V elements. The repeated SL stacks (0.5 μm -thick) and the undoped GaSb buffer layer (0.5 μm -thick) were deposited on GaSb (100) wafers, and several series of 47.0 \AA InAs/21.5 \AA Ga_{0.75}In_{0.25}Sb SL samples were grown over a wide range of Group V flux conditions to preset the growth rates of Group III elements and the V/III flux ratio. To grow the intended ternary structure under minimum cross contamination environment of the Group V fluxes, the V/III flux ratio was set at ~ 3 for both layer depositions, and the growth rates of 1.6 and 0.3 $\text{\AA}/\text{s}$ were used for GaInSb and InAs layers, respectively. The Sb and As cracking zone temperatures were set at 950 $^{\circ}\text{C}$ and 900 $^{\circ}\text{C}$, respectively. Fig. 1 represents a typical strain-balanced ternary structure with an excellent crystalline quality that can be achieved by using the shutter sequence described in the insert of Fig. 1. With a measured period of 68.5 \AA , the grown structure produces a band gap of ~ 45 meV or a corresponding onset wavelength of ~ 27 μm , as demonstrated in the photoresponse (PR) spectrum in Fig. 2.

3. Results and discussions

3.1. Optimization of III/V incorporation

In order to optimize III/V stoichiometry during heteroepitaxy, a first series of ternary SL samples were deposited at 390–450 $^{\circ}\text{C}$ with growth surface temperature (T_g) stepped in approximately 10 $^{\circ}\text{C}$ increments. The growth surface temperatures reported here are pyrometer readings calibrated to the GaSb oxide desorption temperature of 530 $^{\circ}\text{C}$. Since the most obvious effect one would expect from a III/V ratio not equal to one is morphological disorder induced by nucleation and surface defects, we used 50 $\mu\text{m} \times 50 \mu\text{m}$ area scans by AFM to monitor morphological roughness as a function of T_g , with results listed in Table 1. Fig. 3a shows images of a few selected SL samples that were grown at T_g of 390, 400, and 450 $^{\circ}\text{C}$. Despite the large differences in T_g , there were no significant changes in the average root-mean-square (RMS) roughness for the SL samples grown at T_g between 400 and 450 $^{\circ}\text{C}$. In this temperature range, the RMS values were around 3 \AA . However, the RMS roughness value for the SL sample grown at the lowest temperature of 390 $^{\circ}\text{C}$ was significantly different from the others, and was around 21 \AA . Although there were no observable morphological defects for the samples grown at T_g between 400 and 450 $^{\circ}\text{C}$, T_g controls the Group V exchange mechanism that affects the number of Group III antisite defects and optical properties. To study this, the strength of photoresponse (PR) signal was

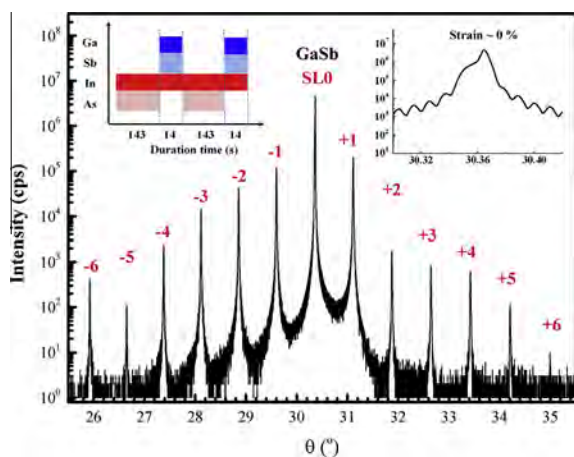


Fig. 1. X-ray diffraction patterns of a 68.0 \AA period superlattice (SL) sample containing a 0.5 μm thick 47.0 \AA InAs/21.5 \AA Ga_{0.75}In_{0.25}Sb SLs. Insert is the shutter sequence employed to create the strain-balanced ternary structure.

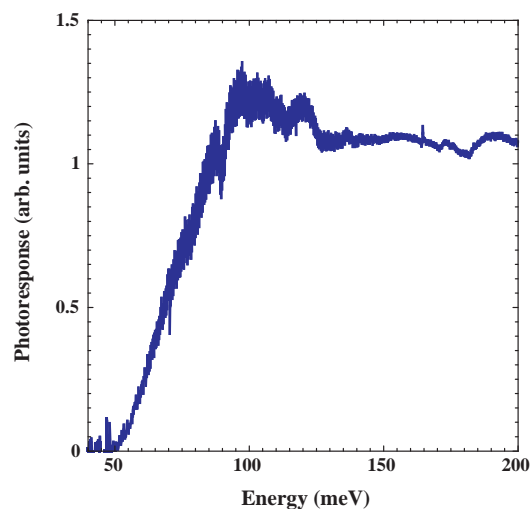


Fig. 2. Photoresponse spectrum at 10 K for the 47.0 \AA InAs/21.5 \AA Ga_{0.75}In_{0.25}Sb superlattices.

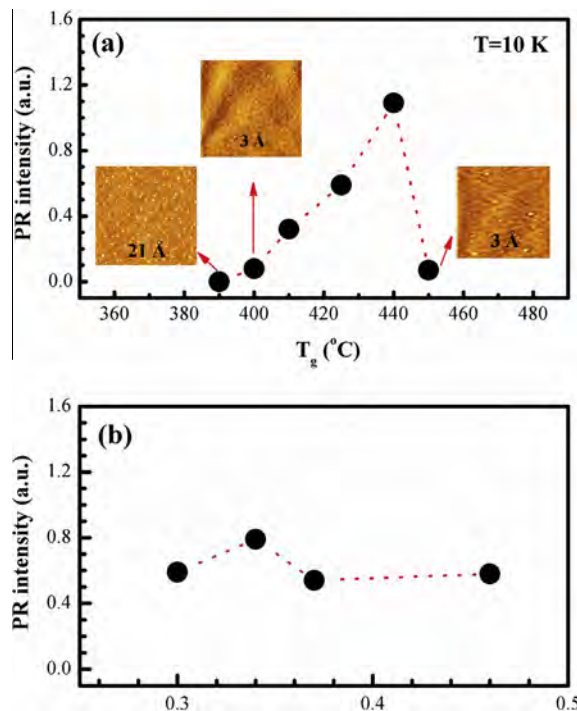


Fig. 3. (a) The 10 K photoresponse (PR) intensity as a function of deposition temperature and (b) As/Sb flux rate. The insert shows AFM images of the 47.0 \AA InAs/21.5 \AA Ga_{0.75}In_{0.25}Sb superlattice samples grown at 390, 400, and 450 $^{\circ}\text{C}$ respectively, the value listed in the bottom of images represents the root-mean-square (RMS) of 50 $\mu\text{m} \times 50 \mu\text{m}$ scans in AFM.

used to check the suitability of a grown material for infrared sensing. The spectra were collected with a Fourier transform infrared spectrometer at a temperature of 10 K. Due to the relatively low resistivity of the samples, the photoconductivity was measured in the current biased mode, with a current of 0.5 mA between two parallel strip contacts on the surface. The five PR spectra were collected from the sample series with T_g varying from 400 to 450 $^{\circ}\text{C}$, where the RMS roughness value was around 3 \AA . Although the PR intensities are given in arbitrary units (a.u.), the relative signal strengths can still be compared as the test conditions for all the samples were kept constant. We observe that the band gap energies of all SLs in this series were around 48 ± 5 meV, while the PR

Table 1

Summary of the measurements results for the sample set. The photoresponse results are from measurements at 10 K. The PR intensity was measured at 100 meV above the band gap. The average root-mean-square (RMS) roughness was based on AFM images of $50 \mu\text{m} \times 50 \mu\text{m}$ area scan. Growth temperature and beam equivalent pressure were noted by T_g and BEP, respectively.

Sample	T_g (°C)	As/Sb (a.u.)	P (Å)	Strain (%)	RMS (Å)	E_g (meV)	PR intensity (arb. units)
SL1	390	0.30	67.8	+0.18	21	X	X
SL2	400	0.30	68.5	+0.17	3	47.0	0.08
SL3	410	0.30	67.5	+0.17	5	43.8	0.32
SL4	430	0.30	68.0	+0.17	5	46.0	0.59
SL5	440	0.30	67.5	+0.16	3	53.0	1.09
SL6	450	0.30	68.6	+0.16	3	50.0	0.07
SL7	430	0.34	68.5	+0.12	3	44.4	0.79
SL8	430	0.37	68.5	+0.02	2	45.3	0.54
SL9	430	0.46	68.1	−0.06	2	47.0	0.58

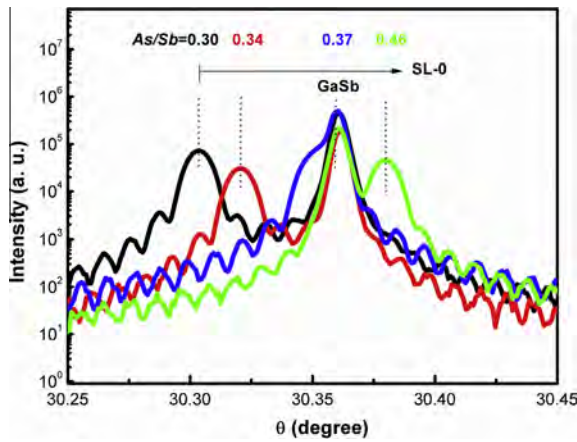


Fig. 4. X-ray diffraction profiles of the (400) reflection showing the GaSb substrate and superlattice peaks.

intensity measured at 100 meV above the band gap gradually increases as T_g increases from 400 to 440 °C. The PR intensity reaches a maximum at 440 °C, and then drops by over an order of magnitude at a higher temperature (see Fig. 3a). Thus, there is a relatively narrow growth window of 410–440 °C for the Group V fluxes and cracking zone temperatures used. Also, an optimized

SL sample produced an overall good photoresponse signal despite the fact that the SL total thickness was only 0.5 μm as demonstrated in Fig. 2. The heavy fringing on the long wavelength portion of the spectrum is not noise but a result of multiple internal reflections through the substrate/buffer/superlattice stack. The lightly n-type GaSb wafers do have significant infrared transparency [8]. This SL has its maximum response over a wide wavelength range up to $\sim 15 \mu\text{m}$. The summary of the results evaluated by HRXRD, AFM and photoconductivity is listed in Table 1.

3.2. Strain balancing process

The next optimization issue needed to be addressed is to prevent the formation of threading dislocations by matching the effective lattice constant of the SL to its substrate, referred to as strain balancing. We selected the SL sample grown at approximately 430 °C from the first study series that has a compressive strain (+0.17%) as the control sample. In order to eliminate compressive strain in this sample, a second series of ternary SL samples were deposited at approximately 430 °C by increasing the As/Sb flux rate ranging from 0.30 to 0.46 in order to form GaAs-like interfaces. We increased the As beam equivalent pressure (BEP) flux from 1.4×10^{-7} to 2.2×10^{-7} torr, while the Sb BEP fixed at 4.8×10^{-7} torr to observe the effect of As/Sb flux on the residual strain and PR intensity. Fig. 4 shows the X-ray diffraction profiles of the (400) reflection from the four samples, where a systematic change in the separation between the substrate and SL peak is observed that

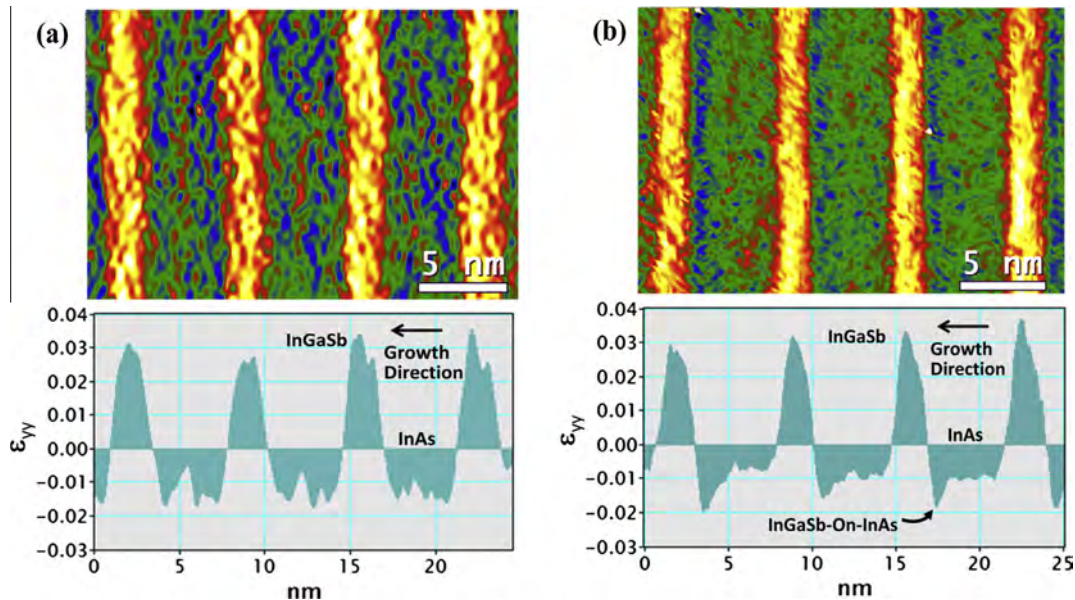


Fig. 5. The strain map (top) and the corresponding strain profile (bottom) of the strain tensor ϵ_{yy} for (a) strained and (b) non-strained InGaSb/InAs superlattices. The profiles are along the growth direction, averaged parallel to the interface over entire strain maps shown on top.

shows that a compressive strain gradually converts to a tensile strain with increasing As/Sb flux ratio. By adjusting the As/Sb flux ratio around 0.37, we were able to completely eliminate 0.17% of compressive strain in the control sample. In order to understand the strain balancing process aberration corrected transmission electron microscopy [9] was used to compare the local strain distribution in the strained control and non-strained samples. The analysis was performed such that the strain component ϵ_{xx} was parallel to the interface (along [011]) and ϵ_{yy} along the growth direction ([100]). For the strained control sample, the GaInSb layers (bright yellow regions) are in strong compressive strain of about +0.03, and the InAs layers (bright green) are in tensile strain of about +0.01. The GaInSb-on-InAs and InAs-on-GaInSb interfaces are seen to exhibit strain inversion, so that the overall strain in these regions is negligible (see Fig. 5a). Further analysis indicated that the net strain over several periods examined is about +0.02, which is close to the measured XRD value of +0.17%. For the non-strained sample, the strain profile in Fig. 5b bottom shows sharp negative spikes at the GaInSb-on-InAs interface corresponding to the dark blue regions in the strain map in Fig. 5b, indicating that this interface is in tensile strain and that its dominant bond type is Ga-As. The corresponding profiles of ϵ_{xx} (not shown) from the same regions in both samples showed negligible values, indicating that the interfaces were coherently matched to the substrate. The net strain examined over several periods was about +0.0005, which is closely lattice matched. The impact of As/Sb flux rate for strain balancing on the PR is plotted in Fig. 3b. The SL grown with ~30% higher As-flux used to balance the strain loses about 17% of the PR signal. Our run-to-run variation of PR intensity is on the order of 10% or less, so the intensity difference between these two samples considered being not significant. Although many engineered interface shutter sequences can be employed [10], the use of As/Sb flux ratio appears to be the simplest way of balancing the strain in this design without losing too much PR intensity. Thus the best quality of materials can be achieved with the simplest shutter sequence described in Fig. 1 insert. The effects of As/Sb flux ratio on the strain and PR intensity are summarized in Table 1.

4. Conclusions

In conclusion, a combination of high-resolution X-ray rocking curve, atomic force microscopy, and photoconductivity measurements was used to tune growth surface condition to stabilize III–V incorporation during MBE growth. For the studies, a series of

47.0 Å InAs/21.5 Å Ga_{0.75}In_{0.25}Sb SLs were deposited at temperature ranging from 410 °C to 450 °C. The results showed that our MBE growth process could produce a band gap around 50 meV. However, the optical quality of the grown samples was very sensitive to growth surface condition. We observed a trend of increasing photoresponse intensity as growth temperature increases. The spectral photoresponse exhibited a strongest signal for the growth temperature of 440 °C, and then rapidly dropped at higher temperatures. The average surface roughness of SL samples that produce strong photoresponse spectra was around 3 Å. A quantitative analysis of the strain distribution performed at the atomic scale by aberration corrected TEM provided valuable information about strain distribution at the interfaces. A strong compressive strain induced by GaInSb alloyed layers could be compensated by tensile strain created by Ga–As bonds at the GaInSb-on-InAs interface along with the InAs layers, which could be accomplished by increasing As/Sb flux ratio.

Conflict of interest

There is no conflict of interest.

Acknowledgements

The work of H.J. Haugan was performed under Air Force contract number FA8650-11-D-5801. The authors thank S. Bowers, G. Landis and A.J. Aronow for a technical assistance with the MBE system and sample preparation for the measurements, respectively.

References

- [1] D.L. Smith, C. Maihiot, *Rev. Mod. Phys.* 62 (1990) 173.
- [2] H. Kroemer, *Physica E* 20 (2004) 196.
- [3] C.H. Grein, W.H. Lau, T.L. Harbert, M.E. Flatté, *Proc. SPIE* 4795 (2002) 39.
- [4] H.J. Haugan, G.J. Brown, S. Elhamri, W.C. Mitchel, K. Mahalingam, M. Kim, G.T. Noe, N.E. Ogden, J. Kono, *Appl. Phys. Lett.* 101 (2012) 171105.
- [5] Heather J. Haugan, Gail J. Brown, Krishnamurthy Mahalingam, Larry Grazulis, Gary T. Noe, Nathan E. Ogden, Junichiro Kono, *J. Vac. Sci. Technol. B* 32 (2014) 2C109.
- [6] Blair C. Connelly, Grace D. Metcalfe, Hongen Shen, Michael Wraback, *Appl. Phys. Lett.* 97 (2010) 251117.
- [7] B.V. Olson, E.A.S.K. Kim, J.F. Klem, S.D. Hawkins, *Appl. Phys. Lett.* 103 (2013) 052106.
- [8] L.P. Allen, P. Flint, G. Dallas, D. Bakken, K. Blanchat, G.J. Brown, S.R. Vangala, W.D. Goodhue, K. Krishnaswami, *Proc. SPIE* 7298 (2009) 72983P.
- [9] K. Mahalingam, H.J. Haugan, G.J. Brown, A.J. Aronow, *Appl. Phys. Lett.* 103 (2013) 211605.
- [10] H.J. Haugan, G.J. Brown, L. Grazulis, *J. Vac. Sci. Technol. B* 29 (2011) 03C101.